Received 4 May 2024; accepted 8 May 2024. Date of publication 10 May 2024; date of current version 31 May 2024.

Digital Object Identifier 10.1109/OJCOMS.2024.3400034

Differential Chaos Shift Keying for FSO Systems: A Novel Approach Under Turbulence and Boresight Pointing Errors

GYAN DEEP VERMA[1], AASHISH MATHUR[1] (Senior Member, IEEE), AND MANAV R. BHATNAGAR[2] (Senior Member, IEEE)

[1]Department of Electrical Engineering, Indian Institute of Technology Jodhpur, Jodhpur 342037, India

[2]Department of Electrical Engineering, Indian Institute of Technology Delhi, New Delhi 110016, India

CORRESPONDING AUTHOR: A. MATHUR (e-mail: aashishmathur@iitj.ac.in)

This work was supported in part by the Science and Education Research Board (SERB), Department of Science and Technology, Government of India under MATRICS Scheme, for the Project "Physical Layer Security Analysis of FSO Communication Systems over Arbitrarily Correlated Channels" under Grant MTR/2023/000473.

ABSTRACT In the last two decades, chaos-based signals have achieved much popularity due to their useful waveform properties such as non-periodicity, wide-band nature, and robustness against eavesdropping by intruders. In this paper, we utilize differential chaos shift keying (DCSK) for free space optical (FSO) communication systems to improve their performance under the combined influence of atmospheric turbulence (AT) and non-zero boresight pointing errors (PEs). We employ the generalized Malaga distribution for modeling the channel gain under all turbulence regimes from weak to strong. Moreover, we utilize the modified Rayleigh distribution to incorporate the effect of jitter and boresight PEs. The computation of the exact average bit error rate (ABER) expression for the proposed FSO system using DCSK is quite tedious. Therefore, we propose two approximations for ABER of the proposed system which show a tight match with the exact analysis and are also valid for the homodyne detection (HMD), heterodyne detection (HD), and intensity modulation/direct detection (IM/DD) techniques. We also observe the impact of different AT parameters (α, β), spreading factor (M), and non-zero boresight PE parameters (k_x, k_y) on the ABER performance of the DCSK-based FSO system. Further, we derive asymptotic ABER expression to obtain insightful observations into the FSO system performance. We also compare the ABER performance of the proposed DCSK-based FSO system with an FSO system employing, correlation delay shift keying (CDSK), binary phase shift keying (BPSK), and code division multiple access (CDMA). We also derive the generalized ergodic capacity (EC) for the considered FSO communication system and show the effect of the spreading factor and boresight on the EC of the DCSK FSO communication system. We derive closed form expression of the average secrecy capacity (ASC) under the combined effect of AT and nonzero boresight PEs for the considered DCSK FSO system.

INDEX TERMS Differential chaos shift keying (DCSK), ergodic capacity (EC), free space optical (FSO), atmospheric turbulence (AT), non-zero boresight, pointing errors (PEs), Malaga distribution, homodyne detection (HMD), heterodyne detection (HD), intensity modulation/direct detection (IM/DD).

I. INTRODUCTION

CISCO annual Internet report (2018–2023) states that there were 4.1 billion Internet users globally in 2018, which is projected to increase to 5.3 billion by 2023 [1]. The unprecedented increment in telecom network data traffic over the past few years has resulted into radio frequency (RF) spectrum congestion. Free space optical (FSO) communication is a promising solution due to its advantages such as high bandwidth, low power consumption, low latency, no electromagnetic interference, unlicensed

© 2024 The Authors. This work is licensed under a Creative Commons Attribution-NonCommercial-NoDerivatives 4.0 License.
For more information, see https://creativecommons.org/licenses/by-nc-nd/4.0/

band, and cost-effectiveness [2], [3], [4], [5], [6], [7], [8], [9], [10]. Optical beams are more collimated and directional compared to their RF counterparts. Hence FSO communication systems are more secure as compared to RF communication systems [4], [5], [7], [8]. However, the optical beam can still be eavesdropped when it gets scattered due to the particles present in the atmosphere in the beam path or when the eavesdropper lies within the field of view of the received beam [4], [5], [8].

Furthermore, there might be a degradation in the FSO communication system performance due to the atmospheric turbulence (AT) present in the channel and pointing errors (PEs) between the received optical beam footprint and the receiver aperture. The primary cause of AT is the presence of temperature gradients in the atmosphere. It arises due to solar heating, wind, clouds, and dust. The AT can significantly affect FSO communication systems by causing random fluctuations in the intensity and phase of the transmitted optical beam. These fluctuations can cause fading and signal distortion, which can lead to a reduction in the performance of the FSO link [3], [4], [8], [9], [10], [17]. The main sources of optical beam misalignment are building sway, thermal expansion, wind load, and weak earthquakes. It results in significant degradation in the FSO communications system performance. The PE consists of two-components; boresight and jitter. Boresight is defined as the fixed displacement between the center of beam foot print and receiver detector, while jitter is the random offset of the beam and receiver detector plane [4], [6], [18], [19], [20]. Other physical obstructions that can temporarily or permanently block the path include birds and trees.

In conventional FSO communication, the intensity modulation/direct detection (IM/DD) technique is very popular [4], [7], [10], [15] because it does not require local oscillator at the receiver that makes the receiver design low cost and easy to implement. The coherent detection techniques are defined based on the local oscillator frequency at the receiver. In HD involves mixing the incoming optical signal with a local oscillator at a different frequency at the photodetector surface. However, in HMD technique, the local oscillator frequency must exactly match the incoming signal. The received instantaneous SNR is proportional to the received optical signal irradiance at the receiver for HD and HMD [4], [21, Eq. (13.16)-(13.17)]. For the IM/DD technique, the received instantaneous SNR is proportional to the square of the received optical signal irradiance at the receiver [4], [7].

Chaos-based communication systems have been widely researched in the past two decades due to the excellent properties of chaos signals such as ease of generation, non-periodicity, sensitivity to initial key value of chaos signal generator, and broadband spectrum [11], [22], [23], [24], [25]. Moreover, chaos signals look like noise which makes them very robust to detect and initial condition sensitivity makes them difficult to regenerate or eavesdrop by the external intruders [26], [27]. The authors in [26], [27], [28] analyzed the physical layer security of spread spectrum and chaos-based modulation schemes where it was observed that the average secrecy capacity of chaos-based schemes was more than the conventional modulation schemes. It was also revealed that DCSK is more secure than the conventional modulation schemes. In direct spread code division multiple access (DS-CDMA), it is a common practice to employ pseudo-noise (PN) sequences. These sequences show strong correlation qualities, however, their primary flaw is their low security. Their short linear complexity allows a linear regression attack to reconstruct them. This limited security can be overcome by using chaotic signals instead of conventional PN sequences, since chaotic signals can be considered as non-periodic signals with an infinite number of states [24]. In [29], the authors showed that the chaotic signals are well suited for multi-user spread-spectrum modulation delivering considerable benefits over conventional modulation systems due to their advantageous wide-band properties. Chaos-based communication systems utilize coherent and non-coherent modulation schemes. Coherent modulation schemes have better average bit error rate (ABER) performance than non-coherent schemes, but chaotic signal synchronization at the receiver during demodulation is challenging in a noisy environment for coherent schemes. Therefore, non-coherent modulation schemes, such as differential chaos shift keying (DCSK) and correlation delay shift keying (CDSK) can be utilized for the FSO communication systems [15], [22], [24], [25], [30]. It was shown in [30] that the ABER performance of DCSK is better than CDSK over an additive white Gaussian noise (AWGN) channel. The authors in [31] showed that DCSK performed better than both direct sequence code division multiple access (DS-CDMA) with imperfect CSI and direct sequence differential phase-shift keying (DS-DPSK).

The authors in [32] derived an approximate ABER performance for single input-single output (SISO) and single input-multiple output (SIMO) DCSK communication systems over Rayleigh fading channel. In [33], the authors experimentally demonstrate a 1 Gbps fiber optic chaos-based communication over 120 km in the metropolitan area network of Athens, Greece. A secure encryption transmission experiment employing a chaotic carrier for 8-Gbps on-off keying (OOK) data over a 10 m FSO communication system is also successfully shown with an ABER below the forward error correction threshold of 3.8×10^{-3} [34]. A self-synchronizing chaotic FSO communication system has been experimentally investigated in the presence of various AT conditions over an approximately 5 km link [13], where the effect of AT has been shown on the ABER performance of chaos-based FSO communication system.

MOTIVATION AND CONTRIBUTIONS

Motivated by above mentioned research works, in this paper, we investigate the ABER performance over an FSO link using DCSK modulation scheme due to the distinct advantages of the DCSK modulation scheme over traditional modulation schemes.

TABLE 1. A comparison of the proposed work with existing related works.

Reference	Year	Channel models	Modulation schemes	Channel Parameters	Detection techniques	Performance metrics
Xia *et al.* [11]	2004	Rayleigh fading	CSK DCSK	—	Coherent non-coherent	ABER
Dawa *et al.* [12]	2020	Nakagami-m	DCSK, QCSK and MC-DCSK	—	Coherent non-coherent	ABER
Rulkov *et al.* [13]	2002	Experimental channel	CPPM	AT	Non-coherent	ABER
Narang *et al.* [14]	2018	Gamma-Gamma	DCSK	AT	Non-coherent	ABER
Narang *et al.* [15]	2023	Gamma-Gamma	DCSK with combining technique	AT	Non-coherent	ABER
Narang *et al.* [16]	2023	Gamma-Gamma	CPWPM	AT	non-coherent	ABER
Proposed Work	—	Malaga (AT) Modified Rayleigh (PE)	DCSK	AT, jitter, and boresight	coherent and non-cohernet	ABER EC, and ASC

Average secrecy capacity (ASC), chaotic pulse position modulation (CPPM), chaos shift keying (CSK), chaotic pulse width position modulation (CPWPM), and multicarrier-DCSK (MC-DCSK)

It is evident from the aforementioned works that the performance of DCSK-based FSO systems over generalized turbulence models has not been considered in literature. The impact of boresight PEs is also ignored in [14], [15] which significantly impacts the performance of FSO systems. We consider a generalized Malaga distribution to model the atmospheric turbulence along the FSO link. Concurrently, the combined effect of jitter and non-zero boresight PEs has been investigated using a modified Rayleigh distribution. In this work, we propose a novel approximation of instantaneous bit error rate (BER) expression for DCSK modulation scheme to investigate the ABER performance of the considered communication system.

To the best of the authors' knowledge, no previous works have considered the scenario of Malaga AT with jitter and boresight to analyze the FSO system performance using DCSK modulation scheme. The main contributions of this paper are summarized as follows:

1) In order to thoroughly evaluate the ABER performance, we propose a novel approximation of the instantaneous BER which shows a tight match with the exact expression [25, Eq. (18)]. We also present a comparison of the instantaneous BER in the existing research works in literature [14], [15] with the proposed approximation.
2) Utilizing the proposed approximation, we analyze the ABER performance of the considered FSO system under the combined impact of AT and non-zero boresight PEs employing DCSK modulation scheme. The derived ABER expressions are generalized and valid for HMD, HD, and IM/DD techniques.
3) Some useful insights into the FSO system performance are obtained through the asymptotic ABER analysis. By utilizing the asymptotic slope, the diversity gain of the considered system is calculated. The diversity gain depends on the considered detection techniques, AT, and non-zero boresight PEs.
4) We derive the generalized ergodic capacity (EC) expression, which includes the combined effects of the generalized Malaga distributed AT, non-zero boresight PE parameters, and generalized detection techniques. An asymptotic expression of the EC is also obtained to observe useful insights in the FSO system performance.
5) We also analyze the physical layer security of the considered DCSK-based FSO communication system in terms of a generalized expression for the average secrecy capacity (ASC) under the combined influence of Malaga distributed AT and nonzero boresight PEs for various detection techniques.
6) We present a thorough investigation of the effect of various system parameters such as detection techniques, AT conditions, spreading factor of DCSK modulation scheme (M), and non-zero boresight PE parameters on the ABER, EC, and ASC of the considered FSO system.

II. SYSTEM DESCRIPTION

Let us present a formal description of the proposed DCSK-based FSO communication system model illustrated in the block diagram in Fig. 1.

A. DCSK MODULATION

We generate DCSK modulated signal using a differential shift keying modulator and a chaotic map to create the chaotic carrier signal. The DCSK modulated sequence consists of two sections; the first is assigned to the reference symbol, and the second is assigned to the data-carrying symbol. If the input data bit is $+1$, then both sections will be the same, whereas if the input data bit is -1, then the reference section is inverted with respect to the data carrying symbol. The modulated information bits are represented as $\mathcal{E}_i \in \{-1, +1\}$, where i is the information bit index. Thus the transmitted symbol $y_{l,i}$ is represented as [24]

$$y_{l,i} = \begin{cases} x_l, & l = 1, 2, 3, \ldots, M \\ \mathcal{E}_i x_{l-M}, & l = M+1, M+2, \ldots, 2M \end{cases} \quad (1)$$

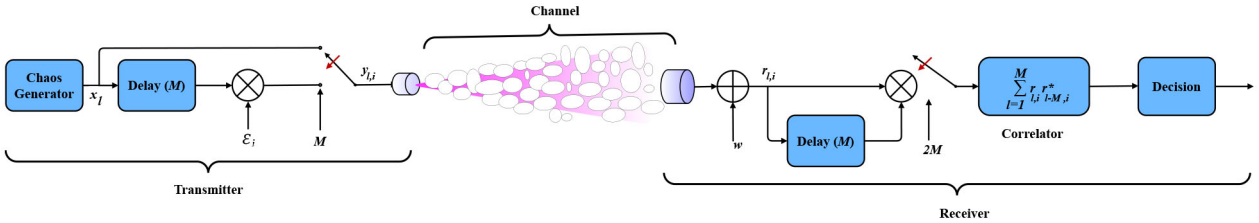

FIGURE 1. Proposed DCSK-based FSO communication system model.

where M represents the spreading factor, x_l denotes the chaotic signal utilized as reference signal, x_{l-M} represents its delayed version used as data-carrying signal, and l denotes the index number of chaotic samples sent for each bit [26], [27], [31].

B. RECEIVED SIGNAL

The received signal at the output of the photodetector is written as

$$r_{l,i} = \eta_0 y_{l,i} I + w_{l,i}, \tag{2}$$

where η_0 is responsivity of the photodetector, $I = I_a I_l I_p$ represents the FSO channel gain where I_a is the Malaga distributed AT [17], I_l represents the deterministic path loss [2], and I_p denotes PE which consists of jitter and non-zero boresight. In (2), $w_{l,i}$ indicates AWGN with zero mean and variance is σ_w^2 [35].

C. AT CHANNEL MODEL

The generalized Malaga distributed AT channel model has attained much popularity over the years due to its ability to capture weak to strong AT regimes. This model includes the effect of three components in the received optical beam: (i) line-of-sight (LoS) component, (ii) coupled-to-LoS component, (iii) off-axis eddies independent scatter component. The probability density function (PDF) of the irradiance due to the Malaga distributed AT along the FSO link is expressed as [17, Eq. (24)]

$$f_{I_a}(I_a) = A \sum_{k=1}^{\beta} a_k I_a^{\frac{\alpha+k-2}{2}} K_{\alpha-k}\left(2\sqrt{\frac{\alpha\beta I_a}{g\beta+\Omega'}}\right), \quad I_a > 0, \tag{3}$$

$$A \triangleq \frac{2\alpha^{\frac{\alpha}{2}}}{g^{1+\frac{\alpha}{2}}\Gamma(\alpha)}\left(\frac{g\beta}{g\beta+\Omega'}\right)^{(\beta+\alpha/2)}, \tag{3a}$$

$$a_k \triangleq \binom{\beta-1}{k-1}\frac{(g\beta+\Omega')^{1-\frac{k}{2}}}{(k-1)!}\left(\frac{\Omega'}{g}\right)^{k-1}\left(\frac{\alpha}{\beta}\right)^{\frac{k}{2}}, \tag{3b}$$

where $K_\nu(.)$ represents the modified Bessel function of second kind and order ν and $\Gamma(.)$ represents the Gamma function. $\alpha > 0$ is the effective number of large scale cells of the scattering process, β is a fading parameter which is a natural number, $2b_0$ represents the average power of the total scatter components, $g = 2b_0(1-\rho)$ indicates the average power of the scattering component received by off-axis eddies, $0 \le \rho \le 1$ is the amount of optical power that is coupled to the LoS component, and Ω' denotes the average power from the coherent component.

D. PE CHANNEL MODEL WITH NON-ZERO BORESIGHT

The Beckmann distribution can approximated into the modified Rayleigh distribution and is given by [19, Eq. (10)]

$$f_U(u) = \frac{u}{\sigma_{mod}^2}\exp\left(-\frac{u^2}{2\sigma_{mod}^2}\right), \quad u \ge 0, \tag{4}$$

where u is the radial displacement vector, which consists of two components, u_x and u_y, representing the horizontal and vertical displacement from the center of the receiver plane, respectively. Both the components are independent and Gaussian distributed, where $u_x \sim N(\kappa_x, \sigma_x^2)$, $u_y \sim N(\kappa_y, \sigma_y^2)$, κ_x and κ_y are horizontal and vertical boresights, σ_x^2 and σ_y^2 denote horizontal and vertical jitters, respectively. The beam width $\Omega_z \approx \theta z$, where θ is divergence angle of the optical beam and z is the distance between transmitter and receiver, $\upsilon = \frac{\sqrt{\pi}R}{\sqrt{2}w_z}$, $A_0 = [\text{erf}(\upsilon)]^2$ is the fraction of the collection power at center of the receiver plane, R is photodetector aperture radius, and $\Omega_{zeq}^2 = \frac{\Omega_z^2\sqrt{\pi}\text{erf}(\upsilon)}{2\upsilon\ \exp(\upsilon^2)}$ denotes the equivalent optical beam radius at the receiver. Further, $\varphi_x = w_{zeq}/(2\sigma_x)$ and $\varphi_y = w_{zeq}/(2\sigma_y)$, $G = \exp(\frac{1}{\varphi_{mod}^2} - \frac{1}{2\varphi_x^2} - \frac{1}{2\varphi_y^2} - \frac{\kappa_x^2}{2\sigma_x^2\varphi_x^2} - \frac{\kappa_y^2}{2\sigma_y^2\varphi_y^2})$, $A_{mod} = A_0 G$, $\sigma_{mod}^2 = (\frac{3\kappa_x^2\sigma_x^4+3\kappa_y^2\sigma_y^4+\sigma_x^6+\sigma_y^6}{2})^{\frac{1}{3}}$, and $\varphi_{mod} = \Omega_{zeq}/(2\sigma_{mod})$. The PDF of PE the random variable (I_p) is expressed as [19]

$$f_{I_p}(I_p) = \frac{\varphi_{mod}^2}{(A_{mod})^{\varphi_{mod}^2}} I_p^{\varphi_{mod}^2-1}, 0 \le I_p \le A_{mod}, \tag{5}$$

E. COMBINED EFFECTS OF AT AND BORESIGHT PE

By utilizing (3) and (5), the generalized PDF of the instantaneous signal-to-noise ratio (SNR) of the received signal is written as [4]

$$f_\gamma(\gamma) = \frac{\varphi_{mod}^2 A}{2^r\gamma}\sum_{k=1}^{\beta} b_k G_{1,3}^{3,0}\left(\begin{matrix}\varphi_{mod}^2+1 \\ \varphi_{mod}^2, \alpha, k\end{matrix}\middle| B\left(\frac{\gamma}{\mu_{r,s}}\right)^{\frac{1}{r}}\right), \tag{6}$$

where $(r=1, s=\sqrt{2})$, $(r=1, s=1)$ and $(r=2, s=1)$ represent the HMD, HD, and IM/DD techniques, respectively [7], [21], [36], $b_k = a_k r^{(\alpha+k-1)}$, $B = \frac{\varphi_{mod}^2\alpha\beta(g+\Omega')}{(\varphi_{mod}^2+1)(g\beta+\Omega')}$, $\mu_{r,s}$ is the average electrical SNR calculated as $\mu_{r,s} = \frac{(s\eta_0\ \mathbb{E}[I])^r}{N_0}$, $\mathbb{E}[I] = \frac{I_l A_{mod}\varphi_{mod}^2(g+\Omega')}{(\varphi_{mod}^2+1)}$, and $\mathbb{E}[.]$ denotes the

expectation operator. In (6) $G_{p,q}^{m,n}(\cdot^{\cdot\cdot\cdot}_{\cdot\cdot\cdot}|\cdot)$ represents the Mejier-G function.

Let us now consider a classical Wyner's wiretap model [37] where the transmitter, Alice (A), wishes to send confidential information to a legitimate receiver, Bob (B), over the considered DCSK-based FSO system with an external eavesdropper (E). The PDF of the instantaneous SNR at B or E can be written in the following alternate form using (6) and [4, Eq. (6)]:

$$f_{\gamma_x}(\gamma_x) = \frac{D_x E_x}{\mu_{r,s}^x} \sum_{k=1}^{\beta_x} b_{kx} G_{r,3r}^{3r,0}\left(\begin{matrix} \mathbf{l_{1x}} - 1 \\ \mathbf{l_{2x}} - 1 \end{matrix} \middle| \frac{E_x\ \gamma_x}{\mu_{r,s}^x} \right), \tag{7}$$

where $x \in \{B, E\}$, $D_x = \frac{\varphi_{mod_x}^2 A_x}{2^r (2\pi)^{r-1}}$, $E_x = B_x^r / r^{2r}$, $\mathbf{l_{1x}} = [\frac{\varphi_{mod_x}^2+1}{r}, \ldots, \frac{\varphi_{mod_x}^2+r}{r}]$ consists of r terms, and $\mathbf{l_{2x}} = [\frac{\varphi_{mod_x}^2}{r}, \ldots, \frac{\varphi_{mod_x}^2+r-1}{r}, \frac{\alpha_x}{r}, \ldots, \frac{\alpha_x+r-1}{r}, \frac{k}{r}, \ldots, \frac{k+r-1}{r}]$ consists of $3r$ terms.

By employing (6), the cumulative distribution function (CDF) of the instantaneous SNR at B and E can be expressed as [4, Eq. (7)]

$$F_{\gamma_x}(\gamma_x) = D_x \sum_{k=1}^{\beta_x} b_{kx} G_{r+1,3r+1}^{3r,1}\left(\begin{matrix} 1, \mathbf{l_{1x}} \\ \mathbf{l_{2x}}, 0 \end{matrix} \middle| \frac{E_x\ \gamma_x}{\mu_{r,s}^x} \right). \tag{8}$$

F. COMPUTATION OF DECISION VARIABLE

In order to retrieve the data bits, we multiply the received signal $r_{l,i}$ and its delayed copy $r_{l-M,i}$. Further, we take the average of resulting sequence over the spreading factor. Therefore, for a given bit i, the decision variable at the correlator's output is expressed as

$$\begin{aligned} D_i &= \mathbb{R}\left(\sum_{l=1}^{M} r_{l,i} r_{l-M,i}^* \right) \\ &= \mathbb{R}\left(\sum_{l=1}^{M} \left(\eta_0 y_{l,i} I + w_{l,i}\right)\left(\eta_0 y_{l-M,i} I + w_{l-M,i}\right)^* \right), \end{aligned} \tag{9}$$

where $\mathbb{R}$ represents real number operator.

III. ABER ANALYSIS

The instantaneous BER expression for the DCSK modulation with the spreading factor M is given by [25, Eq. (17)]

$$P_e(\gamma) = \frac{1}{2}\text{erfc}\left(\sqrt{\frac{\gamma}{4}\left(1 + \frac{M}{2\gamma}\right)^{-1}} \right). \tag{10}$$

The ABER of DCSK modulation with generalized detection technique is written as

$$ABER = \int_0^\infty P_e(\gamma)\, f_\gamma(\gamma) d\gamma. \tag{11}$$

On substituting (6) and (10) in the above expression, it is evident that a tractable closed-form solution is not available. Hence, useful ABER performance design insights for the proposed FSO system cannot be obtained. This motivates us to propose a novel approximation for the instantaneous BER expression for DCSK modulation scheme in (10). We propose the approach in the following subsection:

A. OUR PROPOSED APPROXIMATIONS

1) PRELIMINARIES

Let us consider a non-linear function $f(x)$ which we wish to approximate using another function $g(x)$. If $\mathcal{C}(x)$ represents the error or correction term, then we have:

$$f(x) = g(x) + \mathcal{C}(x). \tag{12}$$

Our objective is to find an accurate approximation of correction term, $\mathcal{C}(x)$, such that the error, $F(x) = f(x) - g(x)$ is minimized in the least square sense. Typically, $\mathcal{C}(x)$ may be a non-linear function of x and a weight vector, $\vec{w}$. The goal of the problem is to find the values of $\vec{w}$ that minimize the sum of the squares of the residuals between $F(x)$ and the predicted values $\mathcal{C}(\vec{w}, x)$. Therefore, this non-linear data fitting problem is mathematically expressed as [38, Appendix D],[39]:

$$\min_{\vec{w}} \|\mathcal{C}(\vec{w}, x) - F(x)\|_2^2 = \min_{\vec{w}} \sum_j \left(\mathcal{C}(w_j, x) - F(x)\right)^2, \tag{13}$$

In order to solve this problem, the following MATLAB command is used:

$$\vec{w} = lsqcurvefit(fun, w_0, xdata, ydata). \tag{14}$$

This command starts at $\vec{w_0}$ and finds coefficients $\vec{w}$ to best fit the nonlinear function fun($\vec{w}$, $xdata$) to the data $ydata$ (in the least-squares sense). For the problem defined in Eq. (13), $fun = \mathcal{C}(\vec{w}, x)$, $xdata = x$, and $ydata = F(x)$.

2) PROPOSED ALGORITHM METHODOLOGY

In line with the aforementioned theory related to non-linear least square data fitting, we propose the following approximation for Eq. (10), for the instantaneous BER of a DCSK-based communication system:

$$P_e(\gamma) \approx P_1(\gamma) + \mathcal{C}(\vec{w}, \gamma), \tag{15}$$

where $P_1(\gamma) = 0.5\text{erfc}(\sqrt{\gamma/4})$ and $\mathcal{C}(\vec{w}, \gamma)$ is a non-linear function of γ that depends on the weight vector $\vec{w}$. Therefore, for our case, the objective function becomes:

$$\begin{aligned} &= \min_{\vec{w}} \|\mathcal{C}(\vec{w}, \gamma) - F(\gamma, M)\|_2^2 \\ &= \min_{\vec{w}} \sum_j \left(\mathcal{C}(w_j, \gamma) - F(\gamma, M)\right)^2, \end{aligned} \tag{16}$$

where M denotes the DCSK spreading factor, $F(\gamma, M) = P_e(\gamma) - P_1(\gamma)$. The MATLAB command to obtain the optimum weight vectors for our case is the following [39]:

$$\vec{w} = lsqcurvefit(\mathcal{C}(\vec{w}, \gamma), w_0, \gamma, F(\gamma, M)).$$

The motivation for the choice of $P_1(\gamma)$ and $\mathcal{C}(\vec{w}, \gamma)$ is described as follows:

a) Choice of $P_1(\gamma)$: $P_1(\gamma) = 0.5\text{erfc}(\sqrt{\gamma/4})$ is chosen in this format to represent the non-linear behavior of erfc(.) in

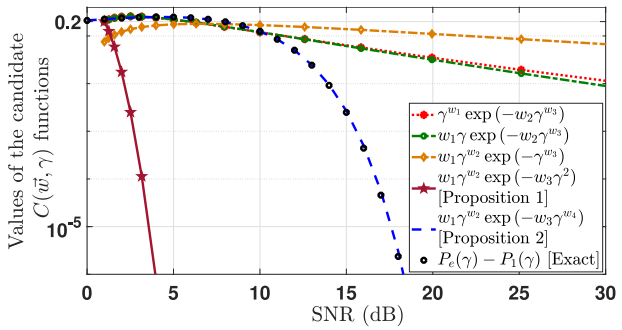

FIGURE 2. Comparison of the accuracy of various candidate $C(\vec{w},\gamma)$ functions with $P_e(\gamma)-P_1(\gamma)$ versus SNR for $M=64$.

the exact expression (10). This term is kept independent of the spreading factor, M, as the average ABER expression for this term can be computed easily and we wanted to keep the dependence on M in the correction term.

b) Choice of $\mathcal{C}(\vec{w},\gamma)$: Since the exact $P_e(\gamma)$ and P_1 are modeled by the erfc$(\cdot)$ function which have a water fall behavior, $\mathcal{C}(\vec{w},\gamma)$ must be chosen such that it emulates this water fall behavior of the erfc$(\cdot)$ function and concurrently minimizes the error $F(\gamma,M)=P_e(\gamma)-P_1(\gamma)$. Some approximations available in literature [40], [41], [42] for modeling the water fall behavior of erfc$(\cdot)$ utilize the weighted sum of exponential functions or a product of an algebraic and exponential functions with appropriate powers and weights. Motivated by this, we propose multiple functions to model the correction term, $\mathcal{C}(\vec{w},\gamma)$ such as, $\gamma^{w_1}\exp(-w_2\gamma^{w_3})$, $w_1\gamma\exp(-w_2\gamma^{w_3})$, $w_1\gamma^{w_2}\exp(-\gamma^{w_3})$, $w_1\gamma^{w_2}\exp(-w_3\gamma^2)$, and $w_1\gamma^{w_2}\exp(-w_3\gamma^{w_4})$. These functions were chosen to be a product of an algebraic function and an exponential function with appropriate powers and weights so that they could follow the water fall behavior of the erfc(.) function in (10). Moreover, the number of weights are chosen so that the power of γ and the weight of γ in the proposed functions are able to mimic $F(\gamma,M)=P_e(\gamma)-P_1(\gamma)$ as closely as possible. We utilized the *lsqcurvefit*$(\cdot,\cdot,\cdot,\cdot)$ command to obtain the optimum weights for each of these candidate $\mathcal{C}(\vec{w},\gamma)$ functions. In Fig. 2, we plot the behavior of these candidates $\mathcal{C}(\vec{w},\gamma)$ functions as a function of SNR for $M=64$. We observe from Fig. 2 that $w_1\gamma^{w_2}\exp(-w_3\gamma^{w_4})$ fit with $P_e(\gamma)-P_1(\gamma)$ better than the other functions. Let us explicitly write the two approximations for the correction term $\mathcal{C}(\vec{w},\gamma)$ as

$$\text{Proposition 1: } \mathcal{C}_1(\vec{w},\gamma)=w_1\gamma^{w_2}\exp\left(-w_3\gamma^2\right), \quad (17)$$

$$\text{Proposition 2: } \mathcal{C}_2(\vec{w},\gamma)=w_1\gamma^{w_2}\exp\left(-w_3\gamma^{w_4}\right), \quad (18)$$

which consist of three (w_1,w_2,w_3) and four (w_1,w_2,w_3,w_4) parameters, respectively.

c) Choice of initial weight vector, $\vec{w}_0$: The initial weight vector for *lsqcurvefit*(.) MATLAB command needs to be real number [38]. The initial weights for the command *lsqcurvefit*(.) should be selected such that the final change in the sum of squares relative to its initial value is less than the default value of the function tolerance which is 10^{-6}. After completion of each run of *lsqcurvefit*(.), a variable "exitflag" returns an integer value which indicates the reason for stopping further iterations of the command. When the function converges to a solution then this variable returns a value of 1, otherwise some other integer value is returned indicating an error [39]. Based on these criteria, for our case, we selected initial weight vector as $\vec{w}_0=[0.205, 0.13, 0.015, 2]$ for our proposed algorithm. This choice of $\vec{w}_0$ resulted in completing optimization because the size of the gradient was less than 10^{-4} times the default value of the function tolerance and the exit flag was 1. It will be revealed in the following section that once we obtain this initial weight vector then our proposed approximation 2, $\mathcal{C}_2(\vec{w},\gamma)$, shows an excellent fit with $P_e(\gamma)-P_1(\gamma)$ for all values of spreading factor, M.

TABLE 2. Optimum weights for $C(\vec{w},\gamma)$ computed using Algorithm 1.

$\mathcal{C}(\vec{w},\gamma)$	M	w_1	w_2	w_3	w_4
$\mathcal{C}_1(\vec{w},\gamma)=w_1\gamma^{w_2}\exp(-w_3\gamma^2)$	16	0.177	-0.016	0.017	-
	32	0.204	0.076	0.013	-
	64	0.225	0.132	0.008	-
$\mathcal{C}_2(\vec{w},\gamma)=w_1\gamma^{w_2}\exp(-w_3\gamma^{w_4})$	16	0.222	0.421	0.285	0.994
	32	0.230	0.420	0.178	1.093
	64	0.238	0.415	0.117	1.136

3) ACCURACY OF THE PROPOSED APPROXIMATIONS

In Fig. 3, we compare our proposed approximations (Proposition 1 and Proposition 2) with the existing approximations in the literature [14, Eq. (20)-(22)] and [15, Eq. (15)-(16)]. The parameters related to the two proposed approximations are mentioned in Table 2. It is observed from Fig. 2 that the existing approximations proposed in literature [14, Eq. (20)-(22)] and [15, Eq. (15)-(16)] for Eq. (10) are very loose for different values of the spreading factor M. We also note that while the proposed approximation 1 (Proposition 1) is having a very close match with the exact results for lower values of M, this approximation becomes inaccurate for larger values of M. However, the proposed approximation 2 fits very accurately with the exact instantaneous BER expression for all values of $M=\{8,16,32,64\}$. The Monte Carlo simulation is performed over 10^8 iterations on MATLAB 2021b on 11^{th} Gen 32.0 GB RAM processor. We have further demonstrated the accuracy of our proposed approximation 2 in Fig. 4 where we compare our proposed approximation 2 with $P_e(\gamma)-P_1(\gamma)$ versus SNR (dB) for different values of DCSK spreading factor (M). It can be noticed that our proposed approximation $\mathcal{C}_2(\vec{w},\gamma)$ shows an excellent fit with $P_e(\gamma)-P_1(\gamma)$, where $P_1(\gamma)=0.5\text{erfc}(\sqrt{\gamma/4})$. A summary of these observations is presented in Table IV for brevity. The parameters related to the two proposed approximations computed using Algorithm 1 are mentioned in Table 2.

Remark 1: Based on Fig. 3 and Table 3, it is revealed that the first proposed method shows high accuracy at

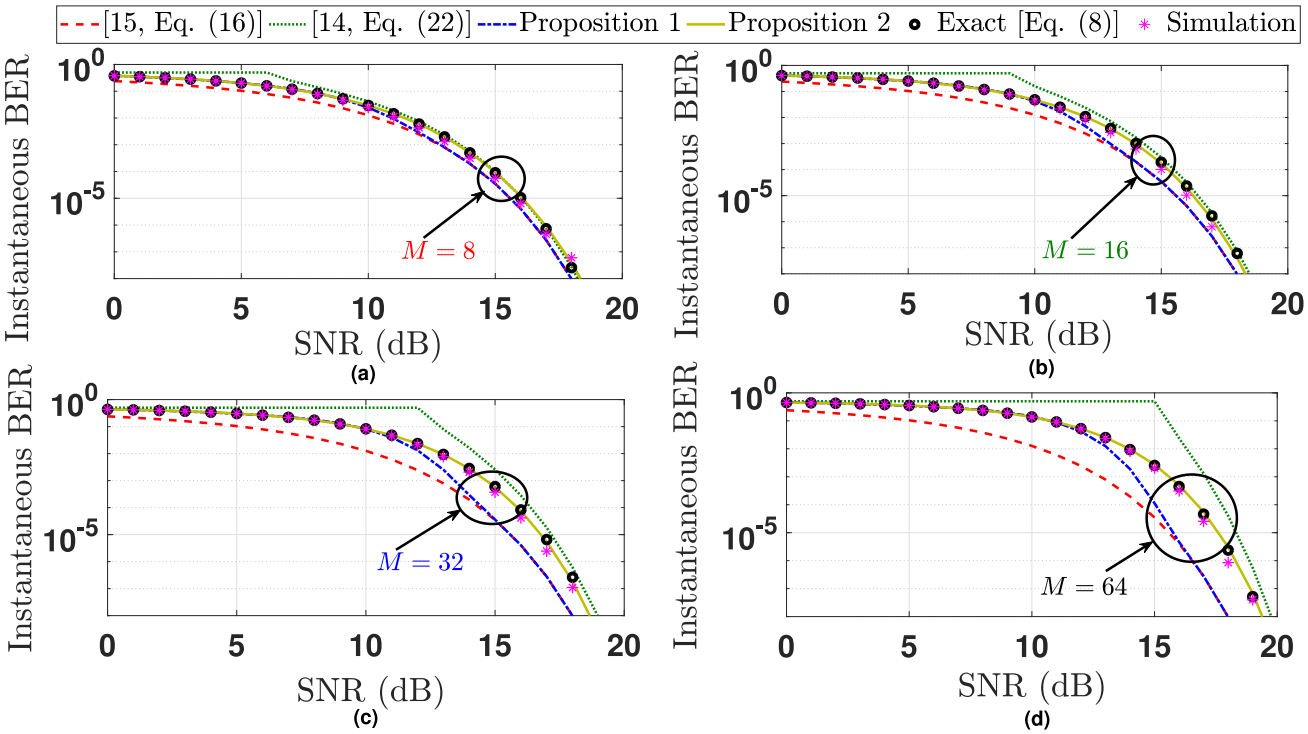

FIGURE 3. Comparison of the existing and proposed approximations with the exact instantaneous BER versus SNR for different spreading factor values and unity channel gain.

Algorithm 1 An Algorithm to Obtain the Optimum Weights for the Correction Terms, $\mathcal{C}(\vec{w}, \gamma)$

Step1→ Compute the numerical value of the exact instantaneous BER, $P_e(\gamma)$, given in (10)
Step2→ Subtract (10) and $P_1(\gamma) = 0.5\text{erfc}(\sqrt{\gamma/4})$ to find $F(\gamma, M) = P_e(\gamma) - P_1(\gamma)$
Step3→ Choose multiple candidate functions for $\mathcal{C}(\vec{w}, \gamma)$.
Step4→ Set initial weight vector, $\vec{w_0}$ and use the MATLAB command *lsqcurvefit*(.) to obtain the optimum weights for each of these candidate $\mathcal{C}(\vec{w}, \gamma)$ functions.
Step5→ Based on the obtained optimum weight vectors of candidate $\mathcal{C}(\vec{w}, \gamma)$ functions, select $\mathcal{C}(\vec{w}, \gamma)$ that closely matches with $F(\gamma, M)$.

lower SNR and at higher SNR shows a poor match with the exact instantaneous BER curve. Since the second proposed approximation shows a very tight match with the exact instantaneous BER expression, we utilize this in the following ABER analysis.

B. DERIVATION OF ABER USING THE PROPOSED APPROXIMATION

Utilizing [43, Eq. (06.27.26.0005.01)], we transform the complementary error function into the Meijer's G function as follows

$$\text{erfc}\left(\sqrt{\frac{\gamma}{4}}\right) = 1 - \frac{1}{\sqrt{\pi}} G_{1,2}^{1,1}\left(\begin{matrix} 1 \\ \frac{1}{2}, 0 \end{matrix} \middle| \frac{\gamma}{4} \right) \tag{19}$$

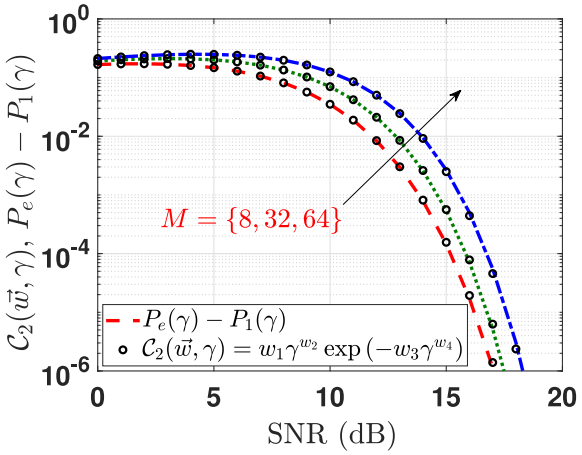

FIGURE 4. Comparison of the accuracy of the proposed approximation 2 with $P_e(\gamma) - P_1(\gamma)$ versus SNR for different $M = \{8, 32, 64\}$.

On substituting (6) and (15) into (11), the ABER is calculated as

$$ABER = 1/2 - J_1 + J_2, \tag{20}$$

where J_1 and J_2 are defined as

$$J_1 = \int_0^\infty \frac{1}{2\sqrt{\pi}} G_{1,2}^{1,1}\left(\begin{matrix} 1 \\ \frac{1}{2}, 0 \end{matrix} \middle| \frac{\gamma}{4} \right) \times \frac{\varphi_{mod}^2 A}{2^r \gamma} \sum_{k=1}^{\beta} b_k G_{1,3}^{3,0}\left(\begin{matrix} \varphi_{mod}^2 + 1 \\ \varphi_{mod}^2, \alpha, k \end{matrix} \middle| B\left(\frac{\gamma}{\mu_{r,s}}\right)^{\frac{1}{r}} \right) d\gamma, \tag{21}$$

TABLE 3. Comparison table of the suggested methods against other proposed methods in the literature.

Reference	Approximation	Remark
[15, Eq. (16)]	$0.5\,\mathrm{erfc}\left(\sqrt{\frac{\gamma}{4}}\right)$	It is valid for $M/(2\gamma) << 1$ and effect of spreading factor has been ignored.
[14, Eq. (22)]	$0.5\,\mathrm{erfc}\left(\sqrt{\frac{\gamma}{4}-\frac{M}{8}}\right)$	It is valid for $M/(2\gamma) << 1$ and convergent for the $\gamma/4 \geq M/8$.
Proposition 1	$0.5\,\mathrm{erfc}\left(\sqrt{\frac{\gamma}{4}}\right)+\mathcal{C}_1(\vec{w},\gamma)$	It contains three parameters and loose match with the exact instantaneous BER.
Proposition 2	$0.5\,\mathrm{erfc}\left(\sqrt{\frac{\gamma}{4}}\right)+\mathcal{C}_2(\vec{w},\gamma)$	It contains four parameters and shows very tight match with exact instantaneous BER.

$$J_2 = \int_0^{\infty} w_1\gamma^{w_2}\exp\left(-w_3\gamma^{w_4}\right) \times\frac{\varphi_{mod}^2 A}{2^r\gamma}\sum_{k=1}^{\beta} b_k G_{1,3}^{3,0}\left(\begin{matrix}\varphi_{mod}^2+1\\ \varphi_{mod}^2,\alpha,k\end{matrix}\middle| B\left(\frac{\gamma}{\mu_{r,s}}\right)^{\frac{1}{r}}\right)d\gamma. \quad (22)$$

Now, using [44, Eq. (2.24.1.1)] in (21), J_1 is solved as

$$J_1 = D_r\sum_{k=1}^{\beta}\frac{b_k r^{\alpha+k-1}}{(2\pi)^{(r-1)}}G_{r+2,3j+1}^{3r+1,1}\left(\begin{matrix}0.5, l_1\\ l_2, 0\end{matrix}\middle|\frac{E_r}{\mu_{r,s}}\right), \quad (23)$$

where $D_r = \frac{\varphi_{mod}^2 A}{2^{2r}\pi^{r-0.5}}$, $E_r = \frac{4B^r}{\mu_{r,s}r^{2r}}$, $l_1 = \frac{\varphi_{mod}^2+1}{r},\ldots,\frac{\varphi_{mod}^2+r}{r}$ consists of r terms, and $l_2 = \frac{\varphi_{mod}^2}{r},\ldots,\frac{\varphi_{mod}^2+r-1}{r},\frac{\alpha}{r},\ldots,\frac{\alpha+r-1}{r},\frac{k}{r},\ldots,\frac{k+r-1}{r}$ includes $3r$ terms. With the help of [43, Eq. (07.34.21.0012.01)], the closed-form expression for Eq. (22) is computed in terms of the H-Fox function as follows:

$$J_2 = G_r\sum_{k=1}^{\beta} b_k H_{1,3}^{3,2}\left(H_r\middle|\begin{matrix}(\varphi_{mod}^2+1,1);\left(1-\frac{w_2}{w_4},\frac{1}{rw_4}\right)\\ (\varphi_{mod}^2,1);(\alpha,1);(k,1)\end{matrix}\right), \quad (24)$$

where $H_{p,q}^{m,n}(\begin{smallmatrix}\cdots\\ \cdots\end{smallmatrix}|\cdot)$ represents the Fox-H function, $G_r = \frac{Aw_1\varphi_{mod}^2}{2^r w_4 w_3^{(w_2/w_4)}}$ and $H_r = \frac{B}{\mu_{r,s}w_3^{\frac{1}{rw_4}}}$.

Remark 2: Observing Eq. (18) and Table 2 allows for the analysis of the impact of the spreading factor (M) on the considered system. From Table 2, it can be seen that for different values of M, we calculate correction terms w_1, w_2, w_3, and w_4. Further, these factors are also involved in Eq (24). Hence, we can conclude that on increasing the value of M, the instantaneous BER performance get degraded. The verification of this tendency in the instantaneous BER curves can also be observed in Fig. 3 (a)-(d) and Fig. 4 as presented in Sections II and VI, respectively.

IV. ASYMPTOTIC ABER ANALYSIS

We investigate the asymptotic behavior of the ABER of the proposed DCSK-based FSO communication system in the high SNR zone to ascertain useful design insights into the system performance comprehensively. To calculate asymptotic ABER expression, we utilize Slater's theorem [45] in (6), to transform the Meijer G-function into the generalized Hypergeometric function as follows [10, Eq. (8)], [46, Eq. (10)]

$$G_{1,3}^{3,0}\left(\begin{matrix}a_1\\ b_1,b_2,b_3\end{matrix}\middle|W\right) = \sum_{h=1}^{3}\frac{\prod_{j=1}^{3}\Gamma\left(b_j-b_h\right)^*}{\Gamma(a_1-a_h)}W^{b_h} \times {}_1F_2\left(1+b_h-c_1;[1+b_h-\mathrm{b}]^*;W\right), \quad (25)$$

where $W = B(\gamma/\mu_{r,s})^{\frac{1}{r}}$ is the argument of the Meijer G-function in Eq. (6), $a_1 = \varphi_{mod}^2+1$, and $b = [b_1,b_2,b_3]=[\varphi_{mod}^2,\alpha,k]$ is a row vector, $(\cdot)^*$ depicts that the index $j=h$ of vector element b will be ignored, and ${}_1F_2(.;.;.)$ is the generalized Hypergeometric function. In the high SNR regime, the argument of the Hypergeometric function $W\to 0$ in Eq (25), consequently ${}_1F_2(.;.;W)\to 1$ [47]. Therefore, the asymptotic expression of (6) can be approximated as

$$f_\gamma(\gamma) \approx X_0\gamma^{\frac{\varphi_{mod}^2}{r}-1}+Y_0\gamma^{\frac{\alpha}{r}-1}+Z_0\gamma^{\frac{k}{r}-1}, \quad (26)$$

where

$$X_0 = \frac{\varphi_{mod}^2 A}{2^r}\sum_{k=1}^{\beta} b_k\Gamma\left(\alpha-\varphi_{mod}^2\right)\Gamma\left(k-\varphi_{mod}^2\right)\left(\frac{B^r}{\mu_{r,s}}\right)^{\frac{\varphi_{mod}^2}{r}},$$
$$Y_0 = \frac{\varphi_{mod}^2 A}{2^r}\sum_{k=1}^{\beta} b_k\frac{\Gamma\left(\varphi_{mod}^2-\alpha\right)\Gamma(k-\alpha)}{\Gamma\left(1+\varphi_{mod}^2-\alpha\right)}\left(\frac{B^r}{\mu_{r,s}}\right)^{\frac{\alpha}{r}},$$
$$Z_0 = \frac{\varphi_{mod}^2 A}{2^r}\sum_{k=1}^{\beta} b_k\frac{\Gamma\left(\varphi_{mod}^2-k\right)\Gamma(\alpha-k)}{\Gamma\left(1+\varphi_{mod}^2-k\right)}\left(\frac{B^r}{\mu_{r,s}}\right)^{\frac{k}{r}}.$$

Substituting (15) and (26) into (11), the asymptotic ABER is written as

$$ABER \approx \int_0^{\infty} P_e(\gamma)\,f_\gamma(\gamma)d\gamma \quad (27)$$
$$\approx 1-K_1-K_2 \quad (28)$$

where K_1 and K_2 are defined as

$$K_1 = \int_0^{\infty}\frac{1}{2\sqrt{\pi}}G_{1,2}^{1,1}\left(\frac{\gamma}{4}\middle|\begin{matrix}1\\ \frac{1}{2},0\end{matrix}\right) \times\left(X_0\gamma^{\frac{\varphi_{mod}^2}{r}-1}+Y_0\gamma^{\frac{\alpha}{r}-1}+Z_0\gamma^{\frac{k}{r}-1}\right)d\gamma, \quad (29)$$

$$K_2 = \int_0^{\infty} w_1\gamma^{w_2}\exp\left(-w_3\gamma^{w_4}\right) \times\left(X_0\gamma^{\frac{\varphi_{mod}^2}{r}-1}+Y_0\gamma^{\frac{\alpha}{r}-1}+Z_0\gamma^{\frac{k}{r}-1}\right)d\gamma. \quad (30)$$

By utilizing [43, Eq. (07.34.21.0009.01)] in (29), K_1 is solved as

$$K_1 \approx \tilde{X}_0+\tilde{Y}_0+\tilde{Z}_0, \quad (31)$$

where

$$\tilde{X}_0 = \frac{X_0\Gamma\left(-\varphi_{mod}^2/r + 1/2\right)\Gamma\left(\varphi_{mod}^2/r\right)}{\Gamma\left(1-\varphi_{mod}^2/r\right)}\left(\frac{1}{4}\right)^{\frac{-\varphi_{mod}^2}{r}},$$

$$\tilde{Y}_0 = \frac{Y_0\Gamma(-\alpha/r + 1/2)\Gamma(\alpha/r)}{\Gamma(1-\alpha/r)}\left(\frac{1}{4}\right)^{\frac{-\alpha}{r}},$$

$$\tilde{Z}_0 = \frac{Z_0\Gamma(-k/r + 1/2)\Gamma(k/r)}{\Gamma(1-k/r)}\left(\frac{1}{4}\right)^{\frac{-k}{r}}.$$

Now, using [43, Eq. (06.05.02.0001.01)] in (30), K_2 is obtained as

$$K_2 \approx \tilde{X}_1 + \tilde{Y}_1 + \tilde{Z}_1, \tag{32}$$

where,

$$\tilde{X}_1 = \frac{X_0 w_1}{w_4^{\varphi_{mod}^2/(rw_4)+w_2/w_4+1}}\Gamma\left(\frac{\varphi_{mod}^2}{rw_4} + \frac{w_2}{w_4}\right),$$

$$\tilde{Y}_1 = \frac{Y_0 w_1}{w_4^{\alpha/(rw_4)+w_2/w_4+1}}\Gamma\left(\frac{\alpha}{rd} + \frac{w_2}{w_4}\right),$$

$$\tilde{Z}_1 = \frac{Z_0 w_1}{w_4^{k/(rw_4)+w_2/w_4+1}}\Gamma\left(\frac{k}{rw_4} + \frac{w_2}{w_4}\right).$$

In (28), X_0, Y_0, and Z_0 incorporate the SNR terms $(1/\mu_{r,s})^{\frac{\varphi_{mod}^2}{r}}$, $(1/\mu_{r,s})^{\frac{\alpha}{r}}$, and $(1/\mu_{r,s})^{\frac{k}{r}}$ in the denominator, respectively. As $\mu_{r,s} \to \infty$, the term containing the smallest power of $\mu_{r,s}$ in the ABER expression will dominate. Hence, we observe that the asymptotic slope for this case is $min\{\varphi_{mod}^2/r, \alpha/r, k/r\}$.

Remark 3: It can be observed that the asymptotic slope of the ABER curves depends upon the considered detection techniques, AT, and non-zero boresight PE parameters. The asymptotic slope is independent of the DCSK spreading factor, M. The spreading factor M affects the coding gain through the weights (w_1, w_2, w_3, and w_4).

Remark 4: In order to observe the impact of the PE parameter (φ_{mod}^2) on the ABER performance, we carefully observe (28), (31), and (32). From (31), it can be seen that $\tilde{X}_0$ dominantly depends upon φ_{mod}^2, and it decreases with increase in φ_{mod}^2. Concurrently, it can be observed using (32) that as φ_{mod}^2 increases the value of $\tilde{X}_1$ increases. Owing to this, the value of K_1 dominantly decreases and K_2 slowly increases. Thus, the ABER performance of the considered DCSK-based FSO system improves with the increase in φ_{mod}^2. This analysis is also verified through the numerical results shown in Fig. 6 in Section IV.

Remark 5: From (28)-(32), we can analyze that with the increase in α, the value of K_1 and K_2 increase. In (31)-(32), the terms $\tilde{Y}_0$ and $\tilde{Y}_1$ dominantly depends upon AT parameter α. As α increases, the values of $\tilde{Y}_0$ and $\tilde{Y}_1$ increase which results in an increase in the values of K_1 and K_2. Hence, the value of ABER decreases with the increase in α. This analysis is also confirmed by the numerical plot shown in Fig. 5 in Section IV. A similar theoretical examination may be carried out to assess the impact of other factors on ABER performance.

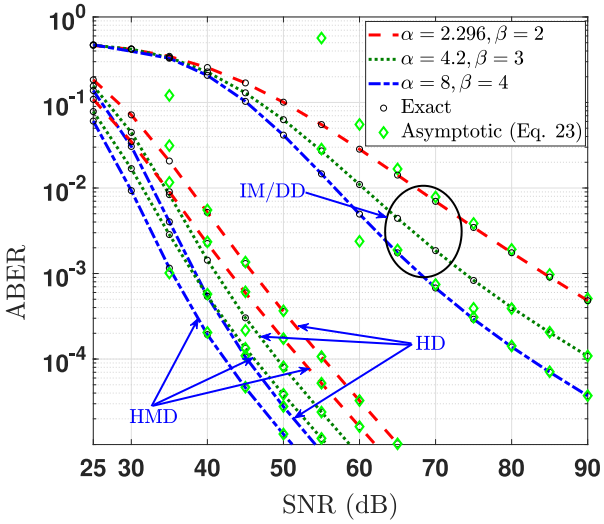

FIGURE 5. Comparison of ABER versus SNR for different turbulence conditions under different detection techniques.

V. EC ANALYSIS

Typically, FSO communication over AT link is characterized by slow-fading channel. The effects of the PEs cause the signal to obliterate at an extremely rapid rate. Due to the fact that the coherence time of the FSO fading channel is of the order of milliseconds, a single fade can flip millions of bits at Gbps data rates. Therefore, the EC analysis is valid in the presence of AT and PEs under the assumption that the duration of the information symbol is sufficient to guarantee the long-term ergodic properties of the turbulence process. The instantaneous capacity of the considered DCSK-based FSO communication system is given by [26, Eq. (8)], [27, Eq. (8)], [28, Eq. (9)], and [31]:

$$C = \log_2\left(1 + \frac{R_D E_b c_{r,s}|I|^r}{N_0}\right) = \log_2\left(1 + \frac{c_{r,s}\,\gamma}{2\,M}\right) \tag{33}$$

where $c_{r,s} = 1$ for HD, $c_{r,s} = \exp/(2\pi)$ for IM/DD, $R_D = 1/T_D = 1/(2MT_c)$ denotes the length of the DCSK frame for each bit, T_c is the chip-time, and $\gamma = (E_b|I|^r)/N_0$. Without loss of generality, we assume T_c to be unity [31]. Using (33), the EC of the considered DCSK-based FSO communication system is written as follows:

$$C_{ec} = \int_0^\infty \log_2\left(1 + \frac{c_{r,s}\,\gamma}{2\,M}\right) \times \frac{\varphi_{mod}^2 A}{2^r\gamma}\sum_{k=1}^{\beta} b_k G_{1,3}^{3,0}\left(\begin{matrix}\varphi_{mod}^2+1\\ \varphi_{mod}^2, \alpha, k\end{matrix}\middle| B\left(\frac{\gamma}{\mu_{r,s}}\right)^{\frac{1}{r}}\right)d\gamma. \tag{34}$$

With the aid of [43, Eq. (07.34.03.0456.01)], we rewrite (34) as follows

$$C_{ec} = \int_0^{\infty} \frac{1}{\log(2)} \mathrm{G}_{2,2}^{1,2}\left[\frac{c_{r,s}\,\gamma}{2\,M}\Big|_{1,0}^{1,1}\right] \times \frac{\varphi_{mod}^2 A}{2^r \gamma} \sum_{k=1}^{\beta} b_k G_{1,3}^{3,0}\left(\begin{matrix}\varphi_{mod}^2+1 \\ \varphi_{mod}^2, \alpha, k\end{matrix}\Big| B\left(\frac{\gamma}{\mu_{r,s}}\right)^{\frac{1}{r}}\right) d\gamma. \quad (35)$$

Now, utilizing [43, Eq. (07.34.21.0013.01)], Eq. (35) can be solved as

$$C_{ec} = \frac{\varphi_{mod}^2 A\; r^{\alpha+k-1}}{\log(2) 2^{2r-1}\pi^{r-1}} \times \sum_{k=1}^{\beta} b_k G_{r+2,3r+2}^{3r+2,1}\left(\begin{matrix}0, 1, \mathbf{l_1} \\ \mathbf{l_2}, 0, 0\end{matrix}\Big| \frac{2\;M\;B^r}{r^{2r} c_{r,s}\mu_{r,s}}\right), \quad (36)$$

where $\mathbf{l_1}$ and $\mathbf{l_2}$ are defined in Eq. (23).

VI. ASYMPTOTIC EC ANALYSIS

For the asymptotic EC analysis, we first expand the Meijer-G function in (36) in terms of the generalized Hypergeometric function [10, Eq. (8)], [46, Eq. (10)] using the Slater's theorem [45]. We observe that the argument of the generalized Hypergeometric function, $\mathcal{W} \to 0$ in the high SNR regime as $\mu_{r,s} \to \infty$. Then with the aid of [46, Eq. (10)], we write the asymptotic expression of EC as follows:

$$C_{ec} = \frac{\varphi_{mod}^2 A\; r^{\alpha+k-1}}{\log(2) 2^{2r-1}\pi^{r-1}} \sum_{k=1}^{\beta} b_k \times \sum_{h=1}^{3r+2} \frac{\prod_{j=1}^{3r+2} \Gamma\left(\mathbf{l_{4_j}} - \mathbf{l_{4_h}}\right)^* \Gamma\left(1 + \mathbf{l_{4_h}} - \mathbf{l_{3_j}}\right)}{\prod_{j=2}^{r+2} \Gamma\left(\mathbf{l_{3_j}} - \mathbf{l_{4_h}}\right)} \mathcal{W}^{\mathbf{l_{4_h}}}, \quad (37)$$

where $\mathcal{W} = \frac{2\;M\;B^r}{r^{2r}\mu_{r,s}}$, $\mathbf{l_3}$=[0, 1, $\frac{\varphi_{mod}^2+1}{r}, \ldots, \frac{\varphi_{mod}^2+r}{r}$] consists of $r+2$ terms, $\mathbf{l_4} = [\frac{\varphi_{mod}^2}{2}, \ldots, \frac{\varphi_{mod}^2+r-1}{r}, \frac{\alpha}{r}, \ldots, \frac{\alpha+r-1}{r}, \frac{k}{r}, \ldots, \frac{k+r-1}{r}, 0, 0]$ consists of $3r+2$ terms. Thus, under high SNR scenario, as $\mu_{r,s} \to \infty$, the smallest power of $\mu_{r,s} \to \infty$ in (37) will dominate. Therefore, the asymptotic slope of EC is $min\{\varphi_{mod}^2/r, \alpha/r, k/r\}$, which is in line with the asymptotic ABER analysis in Section IV

Remark 6: Let us observe the impact of the PE parameter (φ_{mod}^2) on EC of the considered DCSK-based FSO system. With an increase in φ_{mod}^2, the values of ($\frac{2MB}{\mu_{1,s}}$) and ($\frac{\varphi_{mod}^2 A}{2\log(2)}$) increase, while the overall term under Gamma function decreases. Thus, the EC performance improves with the increase in φ_{mod}^2 for the considered DCSK-based FSO system.

Alternatively, to obtain further insights, we utilize a moments-based approach to obtain asymptotic EC expression with the aid of [48, Eq. (8) and (9)]. Thus, the asymptotic EC is written as

$$C_{ec} \approx \log_2\left(\frac{c_{r,s}\mu_{r,s}}{2M}\right) + \epsilon \quad (38)$$

where $\epsilon = \frac{\partial}{\partial n} A F_{\gamma}^{(n)}$ at $n = 0$ with $AF_{\gamma}^{(n)} = \frac{\mathbb{E}[\gamma^n]}{\mathbb{E}[\gamma]^n} - 1$.

We further simplify (38) as follows:

$$C_{ec} \approx \log_2\left(\frac{c_{r,s}\mu_{r,s}}{2M}\right) + \frac{\partial}{\partial n}\left(\frac{\mathbb{E}[\gamma^n]}{\mathbb{E}[\gamma]^n} - 1\right)\Big|_{n=0} = \frac{\partial}{\partial n}\,\mathbb{E}[\gamma^n]\Big|_{n=0}. \quad (39)$$

Now, we use [7, Eq. (20)] into (39) and calculate the first-order derivative of the n^{th} order moment as follows:

$$\frac{\partial}{\partial n}\,\mathbb{E}[\gamma^n] = \frac{r\,\varphi_{mod}^2\,A\,\Gamma(r\,n+\alpha)}{2^r\,\left(r\,n+\varphi_{mod}^2\right)B^{r\,n}} \sum_{k=1}^{\beta} b_m\,\Gamma(r\,n+k) \times \Big\{r\big[\psi(r\,n+\alpha) + \psi(r\,n+k) - \log(B)\big] + \log\left(\frac{c_{r,s}\mu_{r,s}}{2M}\right) - r/\left(r\,n+\varphi_{mod}^2\right)\Big\} \times \left(\frac{c_{r,s}\mu_{r,s}}{2M}\right)^n, \quad (40)$$

where $\psi(.)$ denotes digamma function [42, Eq. (6.3.1)]. Finally, we substitute $n = 0$ in (40) to obtain the asymptotic EC as given below:

$$C_{ec} \approx \frac{rA\Gamma(\alpha)}{2^r} \sum_{k=1}^{\beta} b_k \Gamma(k) \times \Big\{r\left(-1/\varphi_{mod}^2 - \log(B) + \psi(\alpha) + \psi(k)\right) + \log_2\left(\frac{c_{r,s}\mu_{r,s}}{2M}\right)\Big\}. \quad (41)$$

Remark 7: It can be seen from (41) that the asymptotic expression of EC depends upon the FSO system parameters such as the considered detection techniques, AT, and non-zero boresight PE. From (41), we note that the asymptotic EC contains the DCSK spreading factor term (M) in the denominator. Therefore, as the spreading factor M increases, the EC performance degrades. This analysis is also verified through the numerical results shown in Fig. 10.

VII. AVERAGE SECRECY ANALYSIS

In the presence of an active eavesdropper, the maximum rate at which information can be transferred securely to a legitimate receiver is quantified by ASC. The instantaneous secrecy capacity of the considered DCSK-based FSO system is defined as $C(\gamma_B, \gamma_E) = \max\{\log_2(1 + \frac{c_{r,s}\,\gamma_B}{2\,M}) - \log_2(1 + \frac{c_{r,s}\,\gamma_E}{2\,M}), 0\}$. Therefore, the ASC is expressed as

$$\begin{aligned} ASC &= \mathbb{E}\{C(\gamma_B, \gamma_E)\} \\ &= \int_0^{\infty}\int_0^{\infty} C(\gamma_B, \gamma_E) f(\gamma_B, \gamma_E) d\gamma_B d\gamma_E \\ &= \frac{1}{\ln 2}\Bigg[\int_0^{\infty} \ln\left(1 + \frac{c_{r,s}\gamma_B}{2M}\right) f_D(\gamma_D) \int_0^{\gamma_B} f_E(\gamma_E)\, d\gamma_E\, d\gamma_B \\ &\quad - \int_0^{\infty} \ln\left(1 + c_{r,s}\gamma_E\right) f_E(\gamma_E) \int_{\gamma_E}^{\infty} f_B(\gamma_B)\, d\gamma_B\, d\gamma_E\Bigg]. \end{aligned} \quad (42)$$

We re-write Eq. (42) in the following alternative form:

$$ASC = \frac{1}{\ln(2)}(I_1 + I_2 - I_3) \quad (43)$$

where I_1, I_2, and I_3 are defined as follows

$$I_1 = \int_0^\infty \ln\left(1+\frac{c_{r,s}\gamma_B}{2M}\right) f_{\gamma_B}(\gamma_B) F_{\gamma_E}(\gamma_B) d\gamma_B, \quad (44)$$

$$I_2 = \int_0^\infty \ln\left(1+\frac{c_{r,s}\gamma_E}{2M}\right) f_{\gamma_E}(\gamma_E) F_{\gamma_B}(\gamma_E) d\gamma_E, \quad (45)$$

$$I_3 = \int_0^\infty \ln\left(1+\frac{c_{r,s}\gamma_E}{2M}\right) f_{\gamma_E}(\gamma_E) d\gamma_E. \quad (46)$$

Substituting (7) and (8) into (44) and utilizing [44, Eq. (8.4.6.5)], I_1 is obtained as

$$I_1 = D_B D_E \sum_{k=1}^{\beta_B}\sum_{m=1}^{\beta_E} b_{kB} b_{mE} \int_0^\infty G_{2,2}^{1,2}\left(\begin{matrix}1,1\\1,0\end{matrix}\middle|\frac{c_{r,s}\gamma_B}{2M}\right) \times G_{r,3r}^{3r,0}\left(\begin{matrix}\mathbf{l_{1B}}-1\\\mathbf{l_{2B}}-1\end{matrix}\middle|\frac{E_B\gamma_B}{\mu_{r,s}^B}\right) G_{r+1,3r+1}^{3r,1}\left(\begin{matrix}1,\mathbf{l_{1E}}\\\mathbf{l_{1E}},0\end{matrix}\middle|\frac{E_E\gamma_B}{\mu_{r,s}^E}\right) d\gamma_B. \quad (47)$$

Using [43, Eq. (21.02.04.0001)], (47) is evaluated in terms of the extended generalized bivariate Meijer-G function (EGBMF) given by

$$I_1 = D_B D_E \sum_{k=1}^{\beta_B}\sum_{m=1}^{\beta_E} b_{kB} b_{mE} \times G_{3r,r:r+1,3r+1:2,2}^{3r,0:3r,1:1,2}\left(\begin{matrix}\mathbf{l_{2B}}\\\mathbf{l_{1B}}\end{matrix}\middle|\begin{matrix}1,\mathbf{l_{1E}}\\\mathbf{l_{2E}},0\end{matrix}\middle|\begin{matrix}1,1\\1,0\end{matrix}\middle|\frac{E_E\mu_{r,s}^B}{E_B\mu_{r,s}^E},\frac{c_{r,s}\mu_{r,s}^B}{2ME_B}\right). \quad (48)$$

The EGBMF in (48) and (49) is plotted using the MATHEMATICA code provided in [49, Table 2].

Following similar steps for computation of I_1, I_2 is calculated as

$$I_2 = D_B D_E \sum_{k=1}^{\beta_B}\sum_{m=1}^{\beta_E} b_{kB} b_{mE} \times G_{3r,r:r+1,3r+1:2,2}^{3r,0:3r,1:1,2}\left(\begin{matrix}\mathbf{l_{2E}}\\\mathbf{l_{1E}}\end{matrix}\middle|\begin{matrix}1,\mathbf{l_{1B}}\\\mathbf{l_{2B}},0\end{matrix}\middle|\begin{matrix}1,1\\1,0\end{matrix}\middle|\frac{E_B\mu_{r,s}^E}{E_E\mu_{r,s}^B},\frac{c_{r,s}\mu_{r,s}^E}{2ME_E}\right). \quad (49)$$

Finally, I_3 is evaluated by substituting the PDF of γ_E given by (6) into (46) and utilizing [43, Eq. (07).34.16.0001], as follows:

$$I_3 = D_E \sum_{k=1}^{\beta_B} b_{mE} G_{r+2,3r+2}^{3r+2,1}\left(\begin{matrix}0,1,\mathbf{l_{1E}}\\\mathbf{l_{2E}},0,0\end{matrix}\middle|\frac{2ME_E}{c_{r,s}\mu_{r,s}^E}\right). \quad (50)$$

On substituting (48)-(50) into (43), the ASC of the considered system is obtained.

VIII. NUMERICAL RESULTS AND DISCUSSION

In this section, we present a detailed discussion of the analytical results of the proposed DCSK-based FSO communication system. The analytical results are plotted by utilizing the derived expressions presented in the previous section. Further, we thoroughly investigate and discuss the FSO system performance under the effect of various parameters. Unless otherwise stated, the numerical values of the system parameters are set as ($\alpha = 2.296, \beta = 2$), $k_x/R = 1, k_y/R = 2$ $\sigma_x/R = 1, \sigma_y/R = 2$, $M = 16$, $b0 = 0.1079$, $\Omega' = 1.3265$, and $\rho = 0.596$ [4], [7], [8], [17].

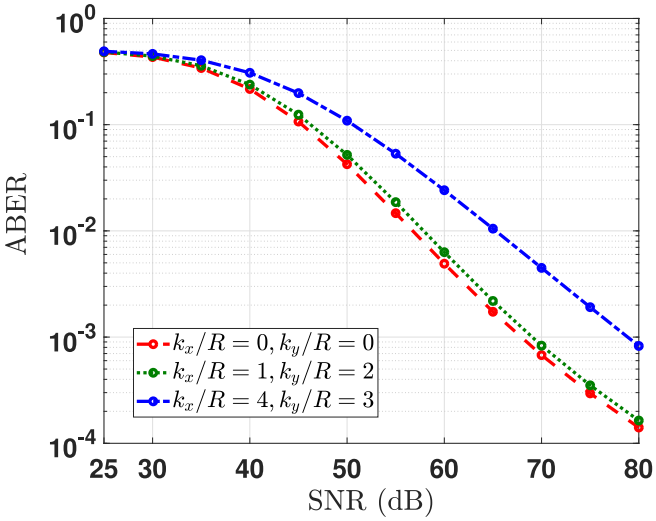

FIGURE 6. Comparison of ABER versus SNR for strong AT using IM/DD detection technique under different boresight conditions.

In Fig. 5, we depict the ABER of the considered FSO system as a function of SNR for different AT scenarios. It is observed that the ABER performance improves on moving from strong (α=2.296; β=2), moderate (α=4.2; β=3), and weak (α=8; β=4) AT condition [7], [8]. As the values of (α, β) are varied from (2.296, 2) to (8, 4), the value of irradiance parameter σ_I^2 decreases from 3.653 to 0.462 resulting in a better ABER performance of the system. This is because of the fact that larger values of σ_I^2 correspond to the case of stronger turbulence. Moreover, it can also be seen that the HMD technique performs better compared to HD and IM/DD techniques. However, one of the main trade-off is the requirement for a local oscillator that is phase-locked with the modulated signal in case of HMD. It is challenging to implement and may lead to stability issues. Additionally, HMD is sensitive to the polarization of the signal, which can introduce errors in the measurement. To obtain some useful insights into the considered FSO system performance, we compute the asymptotic ABER as a function of SNR as depicted in Fig. 5. For strong AT, $M = 16$ and HD technique case, the numerical values of ABER are 3.26×10^{-5} and 3.22×10^{-6} at 60 dB and 70 dB, respectively. The asymptotic slope or diversity gain is calculated as $\log_{10}(3.26 \times 10^{-5})$-$\log_{10}(3.22 \times 10^{-6})$=1.0059 $\approx \min\{\varphi_{mod}^2/r, \alpha/r, k/r\}$. This validates the asymptotic expressions derived in Section III. Following a similar calculation, we can also validate the asymptotic slope for the other curves.

Figure 6 compares the ABER versus SNR for the considered DCSK-based FSO communication system under zero and non-zero boresight conditions. It can be noticed from the figure that as $(k_x/R, k_y/R)$ increases from $(0, 0)$ to

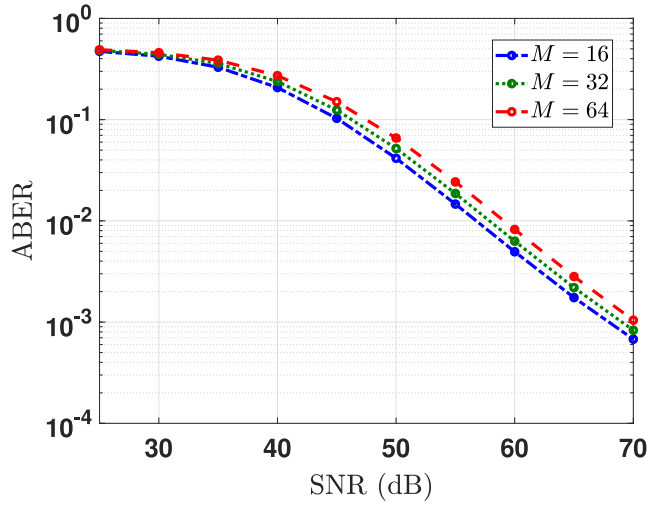

FIGURE 7. Comparison of ABER versus SNR for strong AT and IM/DD detection technique for different spreading factors of DCSK modulation scheme.

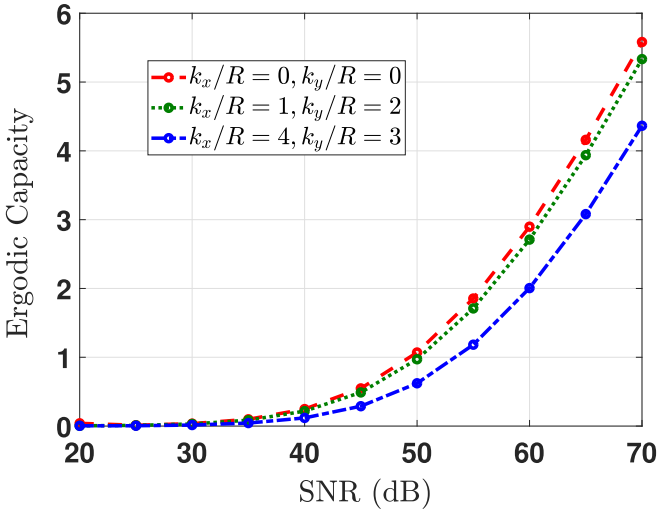

FIGURE 9. Comparison of EC versus SNR for different boresights.

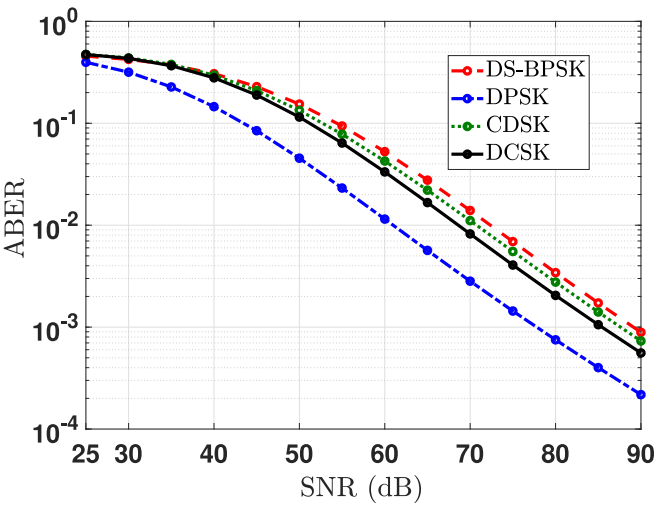

FIGURE 8. Comparison of ABER versus SNR for different modulation schemes.

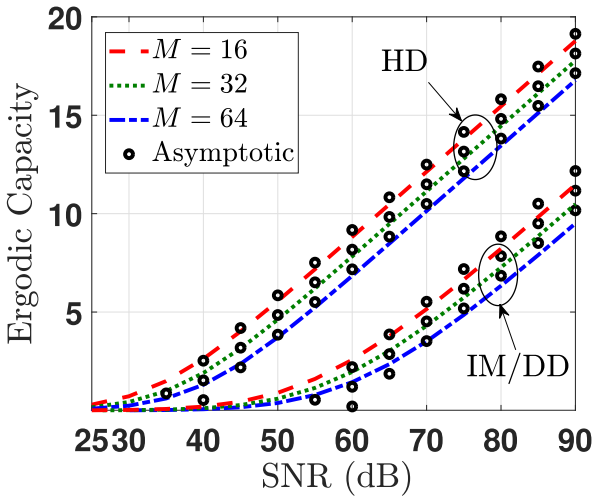

FIGURE 10. Comparison of EC versus SNR for different DCSK spreading factors.

(1, 2) to (4, 3), the ABER performance degrades thereby revealing that the effect of non-zero boresight PEs is quite significant on the FSO system performance. This is due to the misalignment of the laser beam center with respect to the central detector plane, which in turn causes an increase in the fluctuation of the instantaneous SNR.

In Fig. 7, we examine the effect of the DCSK spreading factor (M) on the ABER performance of the proposed FSO communication system. It can be seen from the figure that the ABER performance improves on decreasing the values of M. For the higher value of M, the transmitted signal will be difficult to intercept [26], [27], [50].

In Fig. 8, we compare of ABER as a function of SNR for the different modulation schemes, such as direct spread binary phase shift keying (DS-BPSK), differential phase shift keying (DPSK), CDSK, and DCSK. To obtain these curves, we consider M=32 and IM/DD technique. It can be noticed from the figure that the DCSK modulation scheme outperforms the DS-BPSK and CDSK schemes. It can also be seen that the DPSK scheme performs better than DCSK. However, DPSK is a non-spread spectrum-based keying technique. Therefore, it provides poor data security compared to DCSK.

In Fig. 9, we show a comparison plot of EC versus SNR for the different boresight PE parameters for a fixed, M=32 and IM/DD technique. It can be seen from the figure that as the boresight value increases from (0,0) to (4,3), the EC performance degrades. This occurs due to a misalignment between the center of the laser beam and the receiver detector plane, resulting in an increase in the fluctuation of the instantaneous SNR at the receiver.

Figure 10 presents the EC versus SNR for the different DCSK spreading factors and HD and IM/DD detection techniques. It can be noticed from the figure that EC improves with the increase in SNR. The figure shows that as the value of the DCSK spreading factor (M) decreases, the

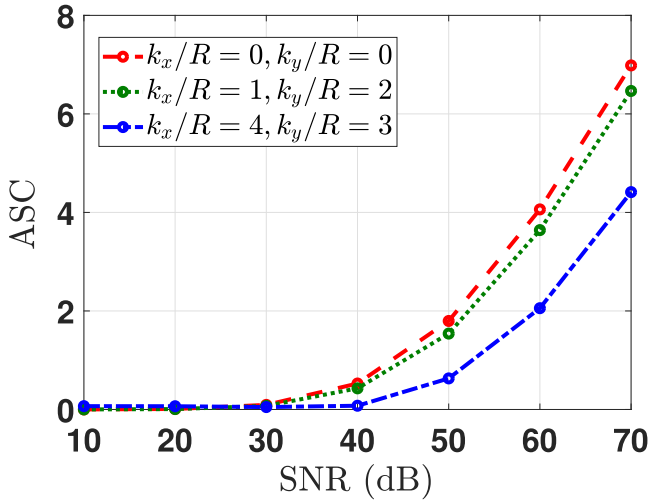

FIGURE 11. Comparison of the ASC versus SNR for different boresight PEs under strong AT with DCSK spreading factor (M=32).

EC performance improves. This observation is also justified through the analysis in Remark 7. This result reveals that the DCSK spreading factor, M plays a crucial role to impact the performance of the DCSK FSO system on the DCSK FSO system. We also note that the asymptotic EC curves match very closely with the analytical EC curves which verifies our asymptotic analysis in Section VI.

In Fig. 11, we compare the effect of the boresight on the ASC of the considered system in the presence of an eavesdropper for fixed jitter $\sigma_x/R = 1$ and $\sigma_y/R = 2$, different boresight PEs $k_x/R, k_y/R = \{0, 0\}$ to $\{4, 3\}$, spreading factor (M=32), strong AT, $\mu_{r,s}^{E} = 15$ dB, and IM/DD technique. It can be noticed that as $k_x/R, k_y/R$ increases the ASC performance degrades. These results show that the effect of nonzero boresight PEs is significant on DCSK-based FSO system secrecy performance.

IX. CONCLUSION AND FUTURE SCOPE

In this research work, we have presented the performance analysis of the FSO-based DCSK communication system, which was evaluated over AT and non-zero boresight PEs. Further, we derived an approximate ABER expression for the proposed system and compared it with the exact expression to verify the accuracy of the derived expressions. The resulting expressions are essential for understanding the effect of distinct AT conditions, detection techniques, and PEs on the performance of DCSK-based FSO systems. We perform an exhaustive asymptotic analysis for the considered communication system. We also analyzed the impact of different spreading factors and non-zero boresight PEs on the EC of considered communication systems. A comprehensive physical layer security analysis of DCSK-based FSO communication systems is not available in literature which will be explored in our future work.

REFERENCES

[1] "Cisco annual Internet report (2018–2023)," Cisco, San Jose, CA, USA, Apr. 2022. https://www.cisco.com/c/en/us/solutions/collateral/executive-perspectives/annual-internet-report/white-paper-c11-741490.pdf

[2] M. A. Khalighi and M. Uysal, "Survey on free space optical communication: A communication theory perspective," *IEEE Commun. Surveys Tuts.*, vol. 16, no. 4, pp. 2231–2258, 4th Quart., 2014.

[3] Z. Ghassemlooy, W. Popoola, and S. Rajbhandari, *Optical Wireless Communications: System and Channel Modelling with MATLAB*. Amsterdam, The Netherlands: CRC Press, 2012.

[4] G. D. Verma, A. Mathur, Y. Ai, and M. Cheffena, "Secrecy performance of FSO communication systems with non-zero boresight pointing errors," *Inst. Eng. Technol. Commun.*, vol. 15, no. 1, pp. 155–162, 2021.

[5] F. J. Lopez-Martinez, G. Gomez, and J. M. Garrido-Balsells, "Physical-layer security in free-space optical communications," *IEEE Photon. J.*, vol. 7, no. 2, pp. 1–14, Apr. 2015.

[6] G. Varotsos, H. Nistazakis, M. Petkovic, G. Djordjevic, and G. Tombras, "SIMO optical wireless links with nonzero boresight pointing errors over M modeled turbulence channels," *Elsevier Optics Commun.*, vol. 403, pp. 391–400, Nov. 2017.

[7] I. S. Ansari, F. Yilmaz, and M. Alouini, "Performance analysis of free-space optical links over Málaga ($\mathcal{M}$) turbulence channels with pointing errors," *IEEE Trans. Wireless Commun.*, vol. 15, no. 1, pp. 91–102, Jan. 2016.

[8] M. J. Saber and S. M. S. Sadough, "On secure free-space optical communications over Málaga turbulence channels," *IEEE Wireless Commun. Lett.*, vol. 6, no. 2, pp. 274–277, Apr. 2017.

[9] Y. Ai, A. Mathur, G. D. Verma, L. Kong, and M. Cheffena, "Comprehensive physical layer security analysis of FSO communications over Málaga channels," *IEEE Photon. J.*, vol. 12, no. 6, pp. 1–17, Dec. 2020.

[10] G. D. Verma and A. Mathur, "Performance improvement of FSO communication systems using hybrid-ARQ protocols," *Appl. Opt.*, vol. 60, no. 19, pp. 5553–5563, Jul. 2021.

[11] Y. Xia, C. Tse, and F. Lau, "Performance of differential chaos-shift-keying digital communication systems over a multipath fading channel with delay spread," *IEEE Trans. Circuits Syst. II, Exp. Briefs*, vol. 51, no. 12, pp. 680–684, Dec. 2004.

[12] M. Dawa, G. Kaddoum, and M. Herceg, "A framework for the lower bound on the BER of DCSK systems over multi-path Nakagami-m fading channels," *IEEE Trans. Circuits Syst. II, Exp. Briefs*, vol. 67, no. 10, pp. 1859–1863, Oct. 2020.

[13] N. Rulkov, M. Vorontsov, and L. Illing, "Chaotic free-space laser communication over a turbulent channel," *Phys. Rev. Lett.*, vol. 89, no. 27, Dec. 2002, Art. no.277905.

[14] G. Narang, M. Aggarwal, H. Kaushal, and S. Ahuja, "The probability of error in FSO communication system using differential chaos shift keying," *Phy. Commun.*, vol. 34, pp. 220–226, Jun. 2019.

[15] G. Narang, M. Aggarwal, H. Kaushal, and S. Ahuja, "Error probability analysis of FSO communication system using differential chaos shift keying," in *Proc. 5th Int. Conf. Signal Proc. Integr. Netw.*, 2018, pp. 452–456.

[16] G. Narang, M. Aggarwal, H. Kaushal, and S. Ahuja, "Error performance analysis for chaotic pulse width position modulation in free space optical communication system," *J. Opt. Commun.*, 2023, to be published. [Online]. Available: https://doi.org/10.1515/joc-2023-0156

[17] A. Jurado-Navas, J. M. Garrido-Balsells, J. F. Paris, A. Puerta-Notario, and J. Awrejcewicz, "A unifying statistical model for atmospheric optical scintillation," *Numer. Simul. Phys. Eng. Process.*, vol. 181, no. 8, pp. 181–205, 2011.

[18] A. A. Farid and S. Hranilovic, "Outage capacity optimization for free-space optical links with pointing errors," *J. Lightw. Technol.*, vol. 25, no. 7, pp. 1702–1710, Jul. 2007.

[19] R. Boluda-Ruiz, A. García-Zambrana, C. Castillo-Vázquez, and B. Castillo-Vázquez, "Novel approximation of misalignment fading modeled by Beckmann distribution on free-space optical links," *Opt. Exp.*, vol. 24, no. 20, pp. 22635–22649, Oct. 2016.

[20] F. Yang, J. Cheng, and T. A. Tsiftsis, "Free-space optical communication with nonzero boresight pointing errors," *IEEE Trans. Commun.*, vol. 62, no. 2, pp. 713–725, Feb. 2014.

[21] J. Senior, *Optical Fiber Communications: Principles and Practice*. Upper Saddle River, NJ, USA: Prentice Hall, 1985.
[22] L. Kocarev, K. S. Halle, K. Eckert, L. O. Chua, and U. Parlitz, "Experimental demonstration of secure communications via chaotic synchronization," *Int. J. Bifurcat. Chaos*, vol. 2, no. 3, pp. 709–713, Sep. 1992.
[23] K. M. Cuomo and A. V. Oppenheim, "Circuit implementation of synchronized chaos with applications to communications," *Phys. Rev. Lett.*, vol. 71, nos. 1–5, p. 65, Jul. 1993.
[24] G. Kaddoum, "Wireless chaos-based communication systems: A comprehensive survey," *IEEE Access*, vol. 4, pp. 2621–2648, 2016.
[25] G. Kaddoum, F. Gagnon, P. Chargé, and D. Roviras, "A generalized BER prediction method for differential chaos shift keying system through different communication channels," *Wireless Pers. Commun.*, vol. 64, no. 2, pp. 425–437, Nov. 2012.
[26] V. Mohan, A. Mathur, and G. Kaddoum, "Analyzing physical-layer security of PLC systems using DCSK: A copula-based approach," *IEEE Open J. Commun. Soc.*, vol. 4, pp. 104–117, 2023.
[27] V. Mohan and A. Mathur, "Secrecy analysis of DCSK-based PLC systems with multiple eavesdroppers," *IEEE Syst. J.*, vol. 17, no. 3, pp. 3646–3657, Sep. 2023.
[28] L. Kong, G. Kaddoum, and M. Taha, "Performance analysis of physical layer security of chaos-based modulation schemes," in *Proc. IEEE 11th Int. Conf. Wireless Mobile Comput., Netw. Commun. (WiMob)*, 2015, pp. 283–288.
[29] F. C. M Lau and C. K. Tse, "Performance analysis methods for non-coherent differential chaos-shift-keying systems," *Chaos-Based Digital Communication Systems*, 1st ed., Berlin, Germany: Springer, 2003.
[30] M. Sushchik, L. Tsimring, and A. Volkovskii, "Performance analysis of correlation-based communication schemes utilizing chaos," *IEEE Trans. Circuits Syst. I, Fundam. Theory Appl.*, vol. 47, no. 12, pp. 1684–1691, Dec. 2000.
[31] G. Kaddoum and N. Tadayon, "Differential chaos shift keying: A robust modulation scheme for power-line communications," *IEEE Trans. Circuits Syst. II, Exp. Briefs*, vol. 64, no. 1, pp. 31–35, Jan. 2017.
[32] S. Mandal and S. Banerjee, "Performance of differential chaos shift keying over multipath fading channels," *IEICE Trans.*, vol. E85-A, no. 1, pp. 2621–2648, 2002.
[33] A. Argyris et al. "Chaos-based communications at high bit rates using commercial fibre-optic links," *Phys. Rev. Lett.*, vol. 438, pp. 343–346, Dec. 2005.
[34] Z. Yiqun et al., "Experimental demonstration of an 8-Gbits free-space secure optical communication link using all-optical chaos modulation," *Opt. Lett.*, vol. 48, pp. 1470–1473, Jun. 2023.
[35] P. Saxena, A. Mathur, M. R. Bhatnagar, and Z. Ghassemlooy, "BER of an optically pre-amplified FSO system under Málaga turbulence, pointing errors, and ASE noise," in *Proc. IEEE 28th Annu. Int. Symp. Pers., Indoor, Mobile Radio Commun.*, 2017, pp. 1–6.
[36] M. Liu, *Principles and Applications of Optical Communications*. Huntersville, NC, USA: Irwin, 1996. [Online]. Available: https://books.google.co.in/books?id=XP5SAAAAMAAJ
[37] A. D. Wyner, "The wire-tap channel," *Bell Syst. Tech. J.*, vol. 54, no. 8, pp. 1355–1387, 1975.
[38] J. Dennis (George Mason Univ., Fairfax, VA, USA). *Nonlinear Least Square Data Fitting*. Apr. 28, 2023. https://math.gmu.edu/ igriva/book/
[39] (MathWorks, Natick, MA, USA). *Solve Nonlinear Curve-Fitting (Data-Fitting) Problems in Least-Squares Sense*. Jan. 2024. https://in.mathworks.com/help/optim/ug/lsqcurvefit.html
[40] M. Chiani, D. Dardari, and M. Simon, "New exponential bounds and approximations for the computation of error probability in fading channels," *IEEE Trans. Wireless Commun.*, vol. 2, no. 4, pp. 840–845, Jul. 2003.
[41] I. M. Tanash and T. Riihonen, "Global minimax approximations and bounds for the Gaussian q-function by sums of exponentials," *IEEE Trans. Commun.*, vol. 68, no. 10, pp. 6514–6524, Jul. 2020.
[42] M. Abramowitz and I. A. Stegun, *Handbook of Mathematical Functions with Formulas, Graphs, and Mathematical Tables*. New York, NY, USA: Dover, 1964.
[43] "A wolfram Web resource." Accessed: Apr. 10, 2024. [Online]. Available: https://functions.wolfram.com/
[44] A. Prudnikov, Y. Brychkov, and O. Marichev, *Integrals and Series. Volume 3: More Special Functions*. Amsterdam, The Netherlands: Gordon Breach Sci. Publ., 1989.
[45] K. Roach, "Meijer-G function representations," in *Proc. Int. Symp. Symb. Algebr. Comput.*, New York, NY, USA, 1997, pp. 205–211. [Online]. Available: https://doi.org/10.1145/258726.258784
[46] M. R. Bhatnagar and Z. Ghassemlooy, "Performance analysis of gamma–gamma fading FSO MIMO links with pointing errors," *J. Lightw. Technol.*, vol. 34, no. 9, pp. 2158–2169, May 1, 2016.
[47] (MathWorks, Natick, MA, USA). *Hypergeometric Function for Numeric and Symbolic Arguments*. Accessed: Apr. 13, 2023. [Online]. Available: https://in.mathworks.com/help/symbolic/hypergeom.html
[48] F. Yilmaz and M.-S. Alouini, "Novel asymptotic results on the high-order statistics of the channel capacity over generalized fading channels," in *Proc. IEEE 13th Int. Workshop Signal Process. Adv. Wireless Commun. (SPAWC)*, 2012, pp. 389–393.
[49] I. S. Ansari, S. Al-Ahmadi, F. Yilmaz, M.-S. Alouini, and H. Yanikomeroglu, "A new formula for the BER of binary modulations with dual-branch selection over generalized-k composite fading channels," *IEEE Trans. Commun.*, vol. 59, no. 10, pp. 2654–2658, Jul. 2011.
[50] G. Narang, M. Aggarwal, H. Kaushal, and S. Ahuja, "Enhancing the security of free space optical communication system by employing chaos-based modulation scheme," *J. Opt. Commun.*, 2023, to be published.